Journal Pre-proofs

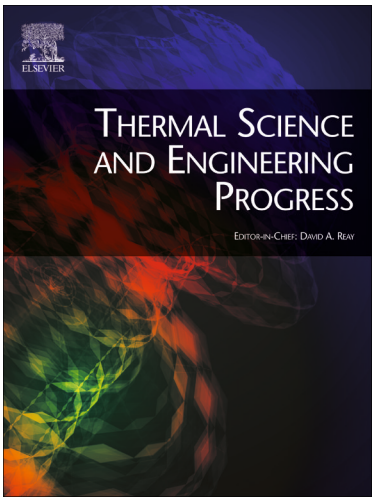

Thermo-magnetic-fluid dynamics analysis of an OsNAN distribution transformer cooled with mineral oil and biodegradable esters

L. Garelli, G.A. Ríos Rodriguez, K. Kubiczek, P. Lasek, M. Stepien, J. Smolka, M. Storti, F. Pessolani, M. Amadei

PII: S2451-9049(21)00023-8
DOI: https://doi.org/10.1016/j.tsep.2021.100861
Reference: TSEP 100861

To appear in: *Thermal Science and Engineering Progress*

Please cite this article as: L. Garelli, G.A. Ríos Rodriguez, K. Kubiczek, P. Lasek, M. Stepien, J. Smolka, M. Storti, F. Pessolani, M. Amadei, Thermo-magnetic-fluid dynamics analysis of an OsNAN distribution transformer cooled with mineral oil and biodegradable esters, *Thermal Science and Engineering Progress* (2021), doi: https://doi.org/10.1016/j.tsep.2021.100861

This is a PDF file of an article that has undergone enhancements after acceptance, such as the addition of a cover page and metadata, and formatting for readability, but it is not yet the definitive version of record. This version will undergo additional copyediting, typesetting and review before it is published in its final form, but we are providing this version to give early visibility of the article. Please note that, during the production process, errors may be discovered which could affect the content, and all legal disclaimers that apply to the journal pertain.

Journal Pre-proofs

Thermo-magnetic-fluid dynamics analysis of an ONAN distribution transformer cooled with mineral oil and biodegradable esters

Garelli, L.[a], Ríos Rodriguez, G.A.[*,a], Kubiczek, K.[e], Lasek, P.[c], Stepien, M.[c], Smolka, J.[b], Storti, M.[a], Pessolani, F.[d], Amadei, M.[d]

[a]*Centro de Investigación de Métodos Computacionales, CIMEC (UNL - CONICET), Predio CONICET-Santa Fe, Colectora RN 168, El Pozo, 3000 Santa Fe, Argentina*
[b]*Institute of Thermal Technology, Faculty of Energy and Environmental Engineering, Silesian University of Technology, Konarskiego 22, 44-100 Gliwice, Poland*
[c]*Dept. of Power Electronics, Electrical Drives and Robotics, Faculty of Electrical Engineering, Silesian University of Technology, B. Krzywuostego 2, 44-100 Gliwice, Poland*
[d]*Tadeo Czerweny S.A., Bv. Argentino 160 (S2252CMP) Gálvez, Santa Fe, Argentina*
[e]*Dept. of Measurement Science, Electronics and Control, Faculty of Electrical Engineering, Silesian University of Technology, Akademicka 10, 44-100 Gliwice, Poland*

Abstract

This work introduces a coupled electromagnetic, thermal and fluid flow analysis of an oil-natural air-natural distribution transformer in order to study the changes in the heat dissipation performance when a biodegradable ester is used to cool the device instead of mineral oil. The transformer has a rated power of 315 kVA and a voltage ratio of 13.2 kV / 0.4 kV. The heat losses in the magnetic core and the windings are computed with the ANSYS® Maxwell software and they are transferred as volume heat source terms to compute the heat conduction. The natural convection of the fluid flow is taken into account using a temperature-dependent density. The heat conduction through the solid walls and radiators panels are also considered. The thermo-hydraulic problem is solved with the software *Code_Saturne*. Data from experimental tests carried out with mineral oil are used to validate the numerical simulations. Equivalent and anisotropic thermal conductivities in the core and the windings are calculated both with a semi-analytic procedure and finite element simulations to simplify the heat conduction model in the active parts. It is found that, after reaching a steady state, the transformer cooled with the ester shows a temperature difference between specific locations at the top and the bottom higher than that cooled with mineral oil. The Magnetic core and the windings also work

*Centro de Investigación de Métodos Computacionales, CIMEC (UNL - CONICET), Predio CONICET-Santa Fe, Colectora RN 168, El Pozo, 3000 Santa Fe, Argentina.
Tel.: +54 (0) 342 4511594 Fax: +54 (0) 342 4511595

Email address: gusadrr@santafe-conicet.gov.ar (Ríos Rodriguez, G.A.)

hotter when ester is used. Finally, the analysis of the flow through the cooling ducts of the windings confirms that the oil velocity is, on average, 25% higher than the ester one.

Key words: Biodegradable esters, Distribution transformer, ONAN cooling, Thermo-fluid dynamics simulations, Electromagnetic simulations.

Nomenclature

$\boldsymbol{g}$	gravity acceleration vector, m/s^2
$\boldsymbol{q}$	heat flux density vector, W/m^2
$\boldsymbol{U}$	velocity vector, m/s
ΔT_{bot}	temperature increment at the bottom of the external surface of the radiator fins, K (see Fig.13)
ΔT_{core}	average temperature increment at the magnetic core, K
ΔT_{HV}	average temperature increment at the high voltage winding, K
ΔT_{LV}	average temperature increment at the low voltage winding, K
ΔT_{oil_top}	temperature increment of the oil at the top of the tank, K (see Fig.13)
ΔT_{oil}	average oil temperature increment for the complete fluid domain, K
Gr	Grashof number
Nu	Nusselt number
Pr	Prandtl number
Ra	Rayleigh number
Cp	specific heat, J/(kg K)
h	heat transfer coefficient, W/(m^2 K)
k	thermal conductivity, W/(m K)
p	pressure, Pa
Q_t	total power loss, W
T	temperature, K
v_j	volume ratio of material-j in a representative cell

Journal Pre-proofs

Abbreviations

CFD	Computational Fluid Dynamics
EM	Electromagnetic
FEM	Finite Element Method
FVM	Finite Volume Method
HST	Hot Spot Temperature
HV	High Voltage
LV	Low Voltage
ONAN	Oil Natural Air Natural
TOT	Top Oil Temperature

Greek letters

β	Thermal expansion coefficient, 1/K
μ	dynamic viscosity, Pa s
∇	gradient operator
ρ	density, kg/m^3
$\tilde{\rho}(T)$	temperature-dependent density, kg/m^3

Subscripts

θ	tangential direction
$amal$	amalgam of insulation materials between conductors (see Eq.19)
C	copper wire conductor
Ci	copper wire insulation (varnish)
$conv$	convection
ins	insulation matrix between conductors
P	craft paper insulation
r	radial direction
rad	radiation
z	axial direction

Journal Pre-proofs

1. Introduction

Electric transformers are a key component in the transmission and distribution electricity networks. Among them, distribution transformers are the least expensive and most widespread, being usually located within the urban areas. Due to these reasons and also because of minimizing the environmental impact and reducing the fire hazard, it is desirable to shift from the usage of mineral oils to natural or synthetic esters to cool the active parts. Mineral oils have very low level of biodegradability, less than 10% according to the OECD 301 standard, while natural and synthetic esters attain 95% level [1].

On the other hand, esters show better dielectric strength than mineral oils, even at low temperature conditions (e.g. $-50\,^{\circ}$C), which is advantageous during the startup of the transformer. This is partially due to the fact that esters have much higher water saturation point than mineral oils. According to [2], the natural ester Environtemp^{TM} FR3^{TM} water saturation point at $25\,^{\circ}$C is 1000 mg/Kg while for a mineral oil it is 70 mg/Kg. At $-20\,^{\circ}$C the corresponding value for FR3^{TM} is 425 mg/Kg and mineral oils have 8 mg/Kg. Esters also exhibit a fire point which is approximately twice higher than that of mineral oils. For example, according to the ISO 2719 / ASTM D92 test methods, the MIDEL® 7131 synthetic ester has fire point at $316\,^{\circ}$C, the natural ester Environtemp^{TM} FR3^{TM} has fire point at $350\,^{\circ}$C, the MIDEL® eN 1204 natural ester has fire point at $360\,^{\circ}$C, and a typical mineral oil has fire point $170\,^{\circ}$C. This is a great advantage regarding safety because, as previously mentioned, distribution transformers are usually located very close to people, within urban areas. Moreover, the higher water saturation point of the esters helps to extend the life of the paper insulation by 5 to 8 times because the esters can absorb higher moisture content from the paper than mineral oils [2]. As a consequence, according to IEC (60076-14) [3] and IEEE (C157.154) [4] insulation standards, it is expected to achieve the same transformer operative life at a hot spot temperature (HST) $15\,^{\circ}$C to $20\,^{\circ}$C hotter than with mineral oils.

However, the high density and the even higher kinematic viscosity make more difficult to them to flow inside the cooling channels of the windings and magnetic core as well as inside the radiator fins. Regarding density at $20\,^{\circ}$C, MIDEL® eN 1204 and Environtemp^{TM} FR3^{TM} have 920 Kg/m^3, MIDEL® eN 7131 has 970 Kg/m^3 and a mineral oil has 880 Kg/m^3 [5]. Therefore, the density of the esters is approximately 4% higher than for mineral oils, and this increment keeps almost constant for higher temperatures. Moreover, some esters show an increase between 3% to 6% in their heat capacity with respect to mineral oils. However, the most important difference between esters and mineral oils appears in their kinematic viscosity. A natural ester, at low temperatures (i.e., $0\,^{\circ}$C) has a kinematic viscosity $\simeq$ 900% bigger than a mineral oil. This percentage reduces to $\simeq$ 500% at $20\,^{\circ}$C and to $\simeq$ 50% at $100\,^{\circ}$C [6]. Therefore, despite the numerous advantages of natural and synthetic esters compared to mineral oils, they are not as efficient as them to remove the heat from the transformer. As a consequence, it is necessary to analyze the cooling performance of the esters when they are used in electric transformers and particularly in this work, in

distribution transformers.

In the last decades there has been an increasing interest to study the thermodynamic performance of both distribution and power transformers using computational methods. The numerical studies are focused on different aspects of the transformers, like the heat dissipation in the radiators [7, 5, 8] or the windings [9, 10] or the efficiency and layout of the radiators fans in ONAF (oil natural air forced) transformers [11, 12, 13]. Usually, the numerical analyses comprise both thermo-hydraulic network models [14, 15] as well as computational electromagnetic and thermo-hydraulic simulations. Both of them have their highlights and drawbacks, and they can be accurate if properly applied taking into account the kind of expected results (i.e., global variable values or detailed flow characteristics) and the computation time required to get those results. In the work of [16], a thermo-electric axisymmetric model based on FEM simulations is developed to assess the temperature distribution in the magnetic core and the windings of a 40 MVA, 32 kV/11 kV ONAN power transformer filled with mineral oil. The time-dependent simulations are solved with COMSOL Multiphysics® and the geometry of the core and the windings are rather simplified since the cooling channels are not taken into account in the model. Also, the oil inlet velocity and temperature are assumed to be constants, i.e., 15 mm/s and 47 °C. Additionally, in [6] the HST and temperature distribution computed inside a power transformer disk-type winding are compared when mineral oil and natural ester are used as cooling fluid. The computations are realized with COMSOL Multiphysics® conjugate heat transfer module on an axisymmetric model of the winding, setting three different inlet flow rates, i.e. 0.78 kg/s, 0.9 kg/s and 1.0 kg/s, a constant and uniform power loss in the windings and also a constant inlet flow temperature of 46.7 °C. It is shown that HST is 9 °C to 11 °C lower for the lowest flow rate when natural ester is used instead of mineral oil. For the other flow rates, the HST attained with mineral oil is equal to or lower than that obtained with the natural ester.

The thermodynamic performance for both a 16.5 MVA, 66 kV power transformer and a 2.3 MVA, 22 kV distribution transformer are analyzed in [17] by performing 2-D CFD simulations with the software ANSYS® Fluent. The fluid flow between the winding discs of both transformers is due to natural convection. However, in both simulations they are generated setting a working pressure at the inlet boundary of the computational domain. The fluids used as coolant are mineral oil, natural ester and synthetic ester. Top oil temperature (TOT) rise, HST rise and average winding temperature are computed and compared to experimental values, considering an ambient temperature of 20 °C. It is found in both transformers that the flow rate for natural and synthetic esters is reduced 50% (for the power transformer) and 40% (for the distribution transformer) to that obtained with the mineral oil. Hence, the HST is 24% (power transformer) and 14% (distribution transformer) higher than that attained with the mineral oil. Therefore, the HST rise limits are not satisfied when natural ester is used in the power transformer. In the case of the distribution transformer, the TOT attained with the natural ester is 3.8 °C higher than with the mineral oil, while the HST is 7.25 °C higher.

Journal Pre-proofs

In the work of [18] the thermal behavior of a 200 kVA ONAN distribution transformer filled with a methyl ester waste vegetable oil is analyzed. First, the AC breakdown voltage, viscosity, density, thermal conductivity and specific heat for this kind of oils are analyzed and compared to those of natural and synthetic esters as well as mineral oils. Then, a detailed 3-D geometry of the distribution transformer is used to run thermo fluid dynamics simulations with ANSYS® Fluent. Grid convergence is performed based on the average oil temperature value for full load operation of the transformer. The magnetic core and winding losses are obtained from experimental tests and for simplicity in the numerical simulations, they are assumed constants and uniformly distributed on the surfaces of the core and the windings. On the external surfaces of the transformer, appropriate correlations are used to calculate the heat transfer coefficients. The simulations were carried out for 10% and 30% of full loaded condition, since temperature distributions for these conditions were measured with a thermographic camera. Good agreement between the numerical results and experiments were found. It is also concluded from the simulations that the HST attained with the waste vegetable oil is 3 °C lower than that obtained with the mineral oil. Because of its lower viscosity, also the velocity and temperature of the oil flowing between the windings are higher and lower, respectively, for the waste vegetable oil than for the mineral one.

More recently [19], the thermal performance of an oil-filled 630 kVA ONAN transformer is analyzed when a mineral oil and three esters are used as coolant. In that work, COMSOL Multiphysics® is used to solve the coupled laminar flow and heat transfer problem in the windings in order to estimate the TOT and the HST for a 20 minutes time lapse. The flow velocity is imposed at the inlet of the winding oil ducts and the pressure is set null at the outlet. The rated power losses at the windings, magnetic core, as well as the stray losses, are taken from data provided by the manufacturer. Then, the TOT and HST computed with a COMSOL Multiphysics® 3-D model are used as input in a Matlab® model to compute the TOT and HST variations all day long. Afterwards, considering different scenarios of the loading power factor and ambient temperatures, the aging and the loss of life of the transformer are assessed. Also the annual energy losses of the transformer, their cost, and their impact on green-houses gases emissions and corresponding environmental cost are evaluated. They conclude that aging of the transformer is reduced when esters are used instead of mineral oil, for different power factors.

The present work was carried out within the BIOtrafo project [20] of Research and Innovation Staff Exchanges (RISE) under a Marie Sklodowska-Curie collaboration and its aim is to analyze with coupled electromagnetic (EM) and thermo fluid dynamic (CFD) 3-D simulations the changes in the heat dissipation performance of an ONAN distribution transformer when natural esters are used as cooling fluid instead of mineral oils. The emphasis of the work is set, on the one hand, in coupling the 3-D EM model with the 3-D CFD model so that the detailed non-uniform power losses distributions computed in the magnetic core and the windings are used as input in the CFD model, thus increasing the accuracy of the computations if compared to other research works where uniform

Journal Pre-proofs

and constant power losses are used. On the other hand, the 3-D CFD model also aims to increase the accuracy of the results by considering a full representation of the transformer where the non-uniform heat distributions at the magnetic core and the windings are transferred to the oil, then to the walls of the oil tank and finally to the surrounding air. Details like considering each cooling duct through the windings, the staircase shape of the magnetic core and the oil flow inside each radiator fin are taken into account in the CFD model. Conduction, convection and radiation heat transfer mechanisms are also considered. Finally, anisotropic heat conduction in the magnetic core and the windings are used in the simulations.

2. Approach to the work

The distribution transformer is manufactured by Tadeo Czerweny S.A. company, which is one of the industrial partners involved in the BIOtrafo project [20]. The transformer has a rated power of 315 kVA and a voltage ratio of 13.2 kV / 0.4 kV. More technical specifications of the device are introduced in section (3). A distribution transformer is chosen for the study as a first development step of the numerical simulation strategies and tools, because of its simple geometry and reduced size if it is compared to a power transformer. A picture of the machine under study in the production line is presented in Fig. 1.

Figure 1: Picture of the distribution transformer in the production line at Tadeo Czerweny S.A., Argentina. View of the windings, magnetic core, current bars and steel frame.

Special care is taken in different aspects of the problem modelization in order to attain accurate results while maintaining computational costs as low as possible. However, some details in the geometry of the machine have been simplified in the CFD model (e.g. the current bars and the steel frame structure which holds the magnetic core and the windings are not taken into account).

Moreover, one quarter of the full transformer geometry has been considered and appropriate symmetry boundary conditions are applied at the cutting / symmetry planes. Additionally, in order to cut down the computational cost, the air surrounding the transformer is not simulated but appropriate heat transfer coefficients values are used instead. The values of these coefficients are computed as the sum of convective and radiative contributions. At first instance, the value of the convective heat transfer coefficient from the solid surfaces of the radiator fins to the air is taken into account based on the previous numerical and experimental research results with a power transformer working in ONAN mode [8].

On the other hand, to take into account the anisotropic heat conduction in the magnetic core and the windings, equivalent thermal conductivities are computed in section 5.3 following semi-analytic [21] and numerical procedures using the finite element method (FEM) on representative cells or sections. This approach is chosen since it is not possible to represent in the CFD simulations of the windings and magnetic core details like wire conductors (copper), wire insulation (varnish), paper sheets used as conductor separators, oil gaps between the conductors or each steel sheet of the magnetic core.

Regarding the electromagnetic (EM) model, the input data such as nominal power, voltage ratio and windings configurations were provided by Tadeo Czerweny S.A. The power loss distributions in the windings and magnetic core were finally computed using FEM and the software ANSYS® Maxwell as a 3-D steady-state model. These results were further used during the first coupling with the CFD model. The detailed 3-D EM model with its results is introduced in section (4).

On the other hand, section (5) describes the coupling of the EM and CFD models, which is realized by transferring the power loss distributions from the FE mesh used in the EM model to the FV mesh of the CFD model. This is carried out by linear interpolation from the nodal values of the FE mesh to the cell centers of the FV mesh. Since the latter mesh is much finer than the former, the interpolation error is rather small. The implementation of the transfer algorithm is carried out within the Salome [22] platform.

Finally, detailed oil velocity and temperature fields for the complete transformer are presented in section (6), specially inside the oil cooling ducts of the windings and between the windings and the magnetic core. Afterwards, average oil temperature differences with respect to a reference temperature at specific locations at the top and the bottom of the transformer are analyzed and compared to experimental data, both for the mineral oil and the ester. In addition, temperature distribution and averaged temperatures of the windings and the magnetic core are evaluated and compared for both fluids. In order to verify the convergence of the complete EM and CFD coupled models, the power losses computed with them are analyzed and compared to the data provided by the manufacturer. As it is known from practical experience and also from previous numerical research, the oil and winding temperatures obtained in the simulations with natural esters are expected to be higher than those obtained with mineral oils [17].

Journal Pre-proofs

3. Technical specifications of the distribution transformer

The present study is performed on a distribution transformer manufactured by Tadeo Czerweny S.A. company. It has a rated power of 315 kVA with a voltage ratio of 13.2 kV / 0.4 kV and voltage regulation $\pm 2 \times 2.5\%$. The cooling of the device is realized by natural convection both in the oil and the air. The transformer is fitted with 16 fins of 605 mm × 180 mm size and 48 fins of 605 mm × 200 mm size. The internal dimensions of the oil tank are: height 720 mm, length 1255 mm and width 410 mm. The active part is comprised of three high-voltage (HV) / low-voltage (LV) windings. A pressboard insulation is placed between the HV and LV windings, and also between the LV winding and the magnetic core. Longitudinal oil channels are provided in the windings in order to increase their cooling. These channels are made by inserting 4 mm × 4 mm square cross-section pressboard bars or sticks during the manufacturing process, denoted as yellow squares in Fig. 2 (right). These channels are also shown in Fig. 2 (left). The same pressboard bars together with 4 mm thickness pressboard separator sheets are used as insulator between the HV and LV windings. This is also depicted in Fig. 2 (right).

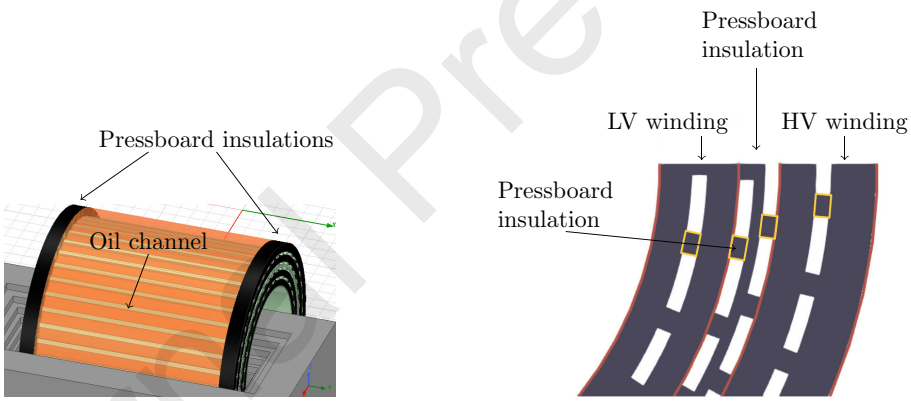

Figure 2: View of the HV and LV windings geometry: detail of the oil channels along the windings (left) and the different insulation materials (right).

The cooling channels have helical shape in the real transformer but they are assumed to be straight in the EM and CFD models in order to simplify the analysis and to reduce computational costs. Circular cross section enameled copper wires are used as conductors in the HV winding, while copper foils are used in the LV one.

The magnetic core is made of 0.27 mm thickness Fe-Si grain oriented electrical steel sheets. A schematic cross section on a plane perpendicular to the symmetry axis of the windings is shown in Fig. 3. Some dimensions of the core cross section are shown in this figure, as well as the layout of the metal sheets. The magnetic core is not manufactured by stacking cut metal sheets of different size (i.e., stacked lamination) but appropriately folding metal sheets instead.

The cores are wounded as loops or strips (two halves with overlapping ends joined together to form a loop in multiple layers of the wound core). This manner of manufacturing the core is taken into account both in the computation of the magnetic fluxes as well as in the calculation of the anisotropic thermal conductivities, as will be later explained in the work.

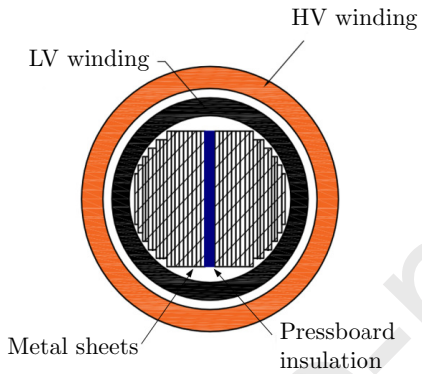

Figure 3: Scheme with cross-section of magnetic core and windings in a normal plane to the windings axis.

It should be mentioned that the pressboard sheets are placed as separator in the gaps between two core loops, so that the oil flow is almost blocked in those regions (see detail in Fig. 3). Moreover, both the bottom and top ends of the windings are insulated with paper sheets and pressboard ribbons. These insulations are shown in color black in Fig. 2(left).

4. Electromagnetic model

The distribution transformer considered in this work has the DYn11 windings configuration. The EM model was prepared in the ANSYS® Maxwell software and it was solved by the iterative *EddyCurrent* 3-D solver. This solver allows for the time-independent, steady-state computations of electromagnetic field distribution. Because of the complex geometry of the windings, particularly the HV one which is composed of many small strands (see Fig. 4), it has to be simplified to carry out the simulations. To this end, an equivalent electrical conductivity is determined assuming that the cross-section of the winding is uniform. Therefore, the copper conductivity is multiplied by coefficients to get the same resistance as in the real winding.

The technical data of the magnetic steel as well as the geometry of the core and the windings were provided by Tadeo Czerweny S.A. The *EddyCurrent* solver allows to compute averaged core loss and ohmic loss per voltage sinusoidal period. This core loss is computed on the basis of the Steinmetz's equation using coefficients calculated from core loss vs. magnetic field characteristics given by

Journal Pre-proofs

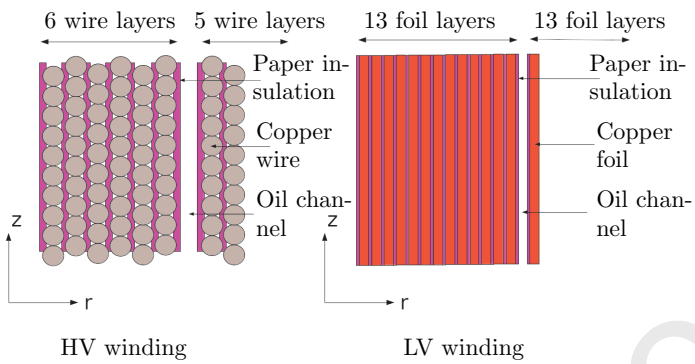

Figure 4: Schematic view of the high (left) and low (right) voltage windings on radial cutting planes.

the device manufacturer. The solver increases the number of mesh elements by 30% in each iteration until the energy percentage error is lower than 1%. The excitation of the primary windings is provided from the external circuit by current sources with amplitudes computed from rated primary voltage and rated power. The secondary windings are connected to resistors with resistances computed from the rated power and the rated secondary voltage to achieve the nominal state of the transformer. The circuits used for the excitation of the coils are presented in Fig. 5.

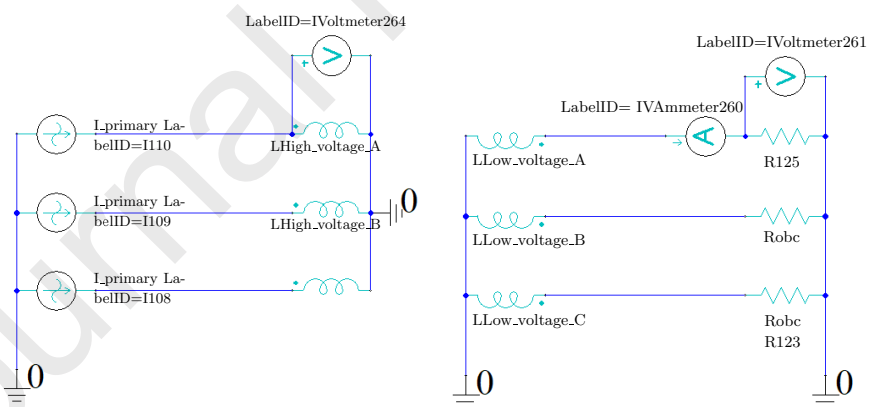

Figure 5: External circuit used as an excitation of primary windings and external resistors used as secondary windings nominal load.

The EM model was validated in two steps. First, a 2-D simplified model was prepared and core loss as well as ohmic loss were computed. The core loss distribution of this 2-D model is presented in Fig. 6.

The results were compared with those given by Tadeo Czerweny S.A. The discrepancy between the power losses was equal to 510 W, which is approxi-

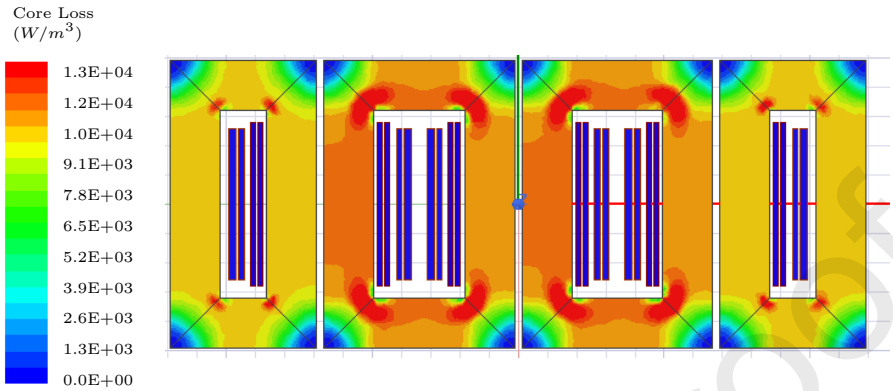

Figure 6: Core loss distribution computed with the 2-D EM model used for validation.

mately 12%, due to many simplifications and assumptions of the 2-D model. The second step of validation was to develop a 3-D model of the transformer. The results of core loss and ohmic loss were again compared with data given by the manufacturer. In this case the discrepancy is equal to 199 W (4.7%) at uniform temperature of 75 °C and 113 W (2.7%) at uniform 70 °C. The 3-D distribution is later used as input data in the CFD models during the first coupling. The magnetic core and windings losses computed with the 3-D EM model are presented in Fig. 7 and Fig. 8, respectively.

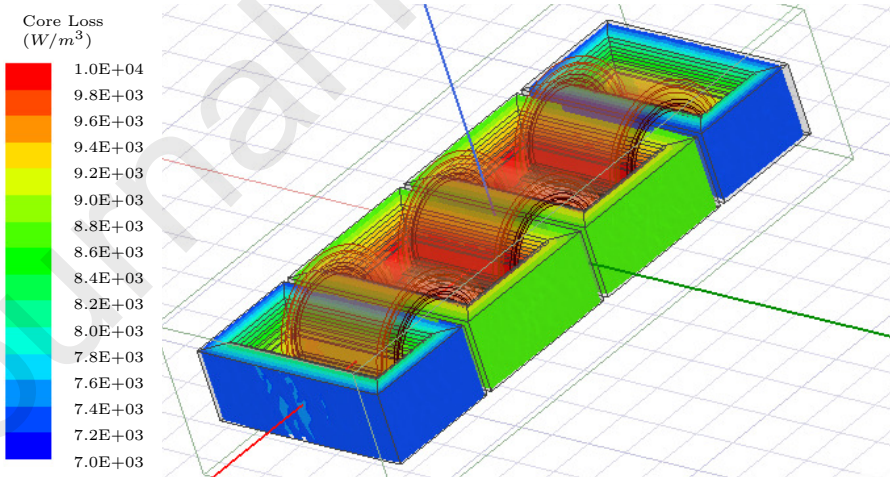

Figure 7: Core loss distribution computed with the 3-D EM model.

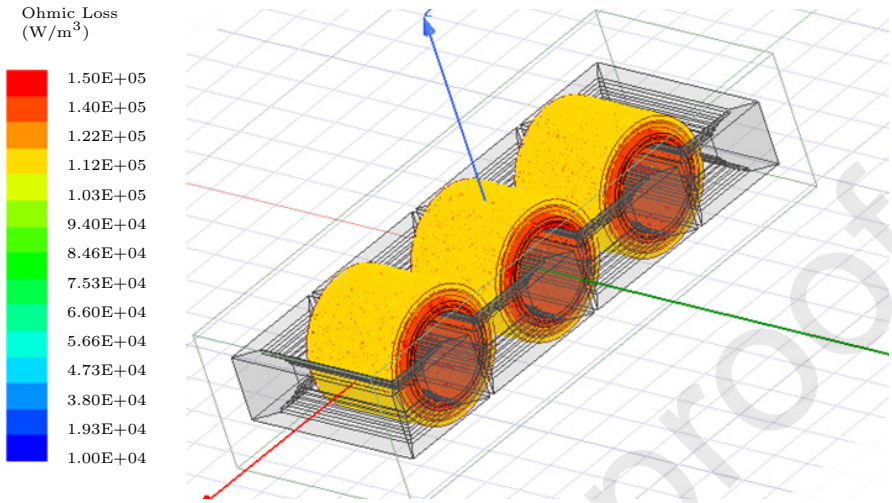

Figure 8: Windings ohmic loss distribution computed with the 3-D EM model.

5. Thermo-hydraulic model

This section first describes the treatment of the transformer geometry within the thermo-hydraulic model and the mesh generation of the magnetic core, windings, fluid and oil tank walls. Then, the governing equations are introduced. The boundary and initial conditions, as well as further assumptions of the model are explained when appropriate. Finally, the computation of equivalent thermal conductivities to consider anisotropic heat conduction in the windings and magnetic core is described.

5.1. Geometry processing and mesh generation

The STEP-format files with the geometries of the different machine parts were provided by Tadeo Czerweny S.A. company. The pre-processing of the geometry, the assignment of the various boundary conditions to the different components of the transformer and the STL mesh generation required by snappyHexMesh [23] were carried out within the Salome [22] platform. The fluid mesh is generated with snappyHexMesh, which is an open-source, fully parallel, cross-platform library for polyhedra mesh generation implemented within the OpenFOAM®framework.

The computational domain used in the simulations considers one quarter of the complete transformer because a high number of cells are required to compute accurate results not only of the global variables of interest (e.g. average oil temperature, average heat transfer coefficients, total dissipated power) but also details of the oil flow and temperature distribution at the entrance and inside the winding channels, in the small gaps between the core and the LV winding

and also inside of each radiator fin. Because one quarter of the complete domain is considered, symmetry boundary conditions are applied at the cutting planes. Fig. 9 shows a picture of the simulation domain.

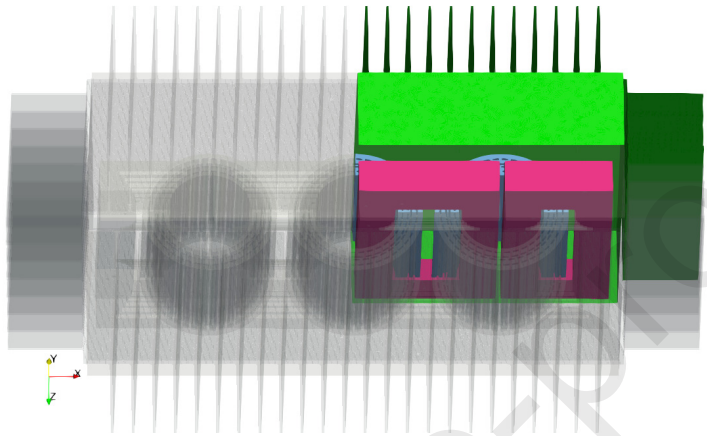

Figure 9: Computational domain (coloured) for the thermo-fluid dynamics simulation with *Code_Saturne*. One quarter of full domain is considered.

The meshes for the fluid, windings and core are made up of polyhedra but they are hexa-dominant. A mesh convergence analysis using meshes of 15, 25 and 35 million cells was carried out. For the mesh with approximately 35 million cells in total, the number of cells used for the core is approximately 3.1 millions and that for the windings is approximately 5.5 millions. The meshes are non-conformal at the interfaces between the fluid and the solids. All the meshes are created in a monolithic way, ensuring that all quality criteria metrics (e.g. non-orthogonality, face skewness) are applied to the whole domain, avoiding quality issues during the mesh joining process at the fluid and solid interfaces.

Moreover, special refinement of the fluid mesh is performed near the solid surfaces in order to accurately solve the thermal and fluid boundary layers and thus the heat transfer between the solids and the fluid. This is particularly important at the oil ducts in the windings, where there are approximately 7 cells along the thickness (4 mm) of the duct. Inside the radiator fins there are 8 cells along the thickness (5 mm) of the fluid mesh. The refined regions are clearly visible in Fig. 10. A cut of the core and windings meshes perpendicular to the axis of the windings can be seen in that figure. The meshes include those of the pressboard sticks used as separators to generate the oil cooling channels and the pressboard insulation between the LV and HV windings.

The windings (light blue) and the magnetic core (red) are also discretized with FV meshes as shown in Fig. 10, where the heat conduction problem is solved. In this case, the heat source values at the centers of each cell are computed by linear interpolation of the non-uniform heat loss distribution computed with the EM model. Since the finite element meshes used to solve the electro-

magnetic problem with ANSYS Maxwell® are much coarser than those of the thermal problem, a linear interpolation algorithm is employed to compute the required values at the cell centers of the FV mesh.

Indeed, Figs 7 and 8 show the power loss distribution computed with the EM numerical model (see Section 4). The total power loss provided in the data sheet of the manufacturer is $Q_{t,Exp} = 4250\,\mathrm{W}$ and that computed with the EM numerical model described in Section 4 at a reference temperature of $75\,^{\circ}\mathrm{C}$ is $Q_{t,EM} = 4449\,\mathrm{W}$. Because one quarter of the transformer is considered in the CFD simulations, the power losses interpolated to the FV mesh of the windings and core of the CFD model are computed as this latter value divided by four, i.e., $1112.25\,\mathrm{W}$. However, because of the errors introduced by the interpolation procedure, the total power interpolated on the FV mesh is equal to $Q_{t,Interp} = 1114\,\mathrm{W}$.

On the other hand, the heat conduction through the steel walls of the external casing and radiators fins is taken into account in the simulations. To this end, a structured mesh for the solid that models these walls is constructed. A cut of this mesh can be observed in Fig. 10. The thermal conductivity of the carbon steel of the fins and the casing is $k_{carbon_steel} = 54\,\mathrm{W/(m\,K)}$ and it is assumed to be isotropic.

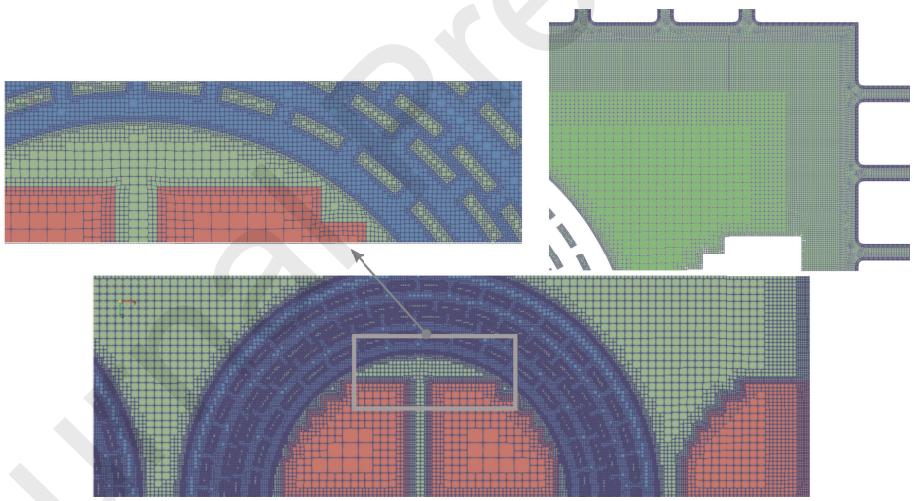

Figure 10: Cut of the fluid and radiator fins meshes. The cutting plane is perpendicular to the axis of the windings (left). Detail of the fluid and the solid meshes at the radiator fins (right).

5.2. Governing equations

The oil natural flow in the tank is governed by the continuity and momentum conservation equations for unsteady incompressible viscous laminar flows of thermally conducting Newtonian fluids. Under these assumptions, the continuity equation is given by the null divergence of the velocity field

$$\nabla \cdot \boldsymbol{U} = 0 \tag{1}$$

where $\boldsymbol{U} = \boldsymbol{U}(x, y, z, t)$ is the flow velocity field and $\nabla = (\partial/\partial x, \partial/\partial y, \partial/\partial z)$ is the gradient operator. On the other hand, the momentum equation is given by

$$\rho \frac{D\boldsymbol{U}}{Dt} = -\nabla p + \tilde{\rho}(T)\boldsymbol{g} + \nabla \cdot (\mu(T)\nabla \boldsymbol{U}) \tag{2}$$

being $D\boldsymbol{U}/Dt$ the material or Lagrangian derivative of the velocity field (namely, $D\boldsymbol{U}/Dt = \partial \boldsymbol{U}/\partial t + (\boldsymbol{U} \cdot \nabla)\boldsymbol{U}$), ∇p is the pressure gradient, $\boldsymbol{g}$ is the gravity vector, $\mu(T)$ is the temperature-dependent dynamic viscosity, $\tilde{\rho}(T) = \rho + \Delta\rho$ is the temperature-dependent density, and ρ is a reference density value. The temperature-dependence of the density is only taken into account in the source term of the momentum equation using the Boussinesq approximation because the density changes are very small ($\Delta\rho/\rho << 0.1$) for the range of the transformer operating temperatures [24]. However, variation of physical properties like the dynamic viscosity, thermal conductivity and specific heat are important [25] within this range, so appropriate functions will be later introduced for these properties as function of the temperature for both the mineral oil and the ester.

Additionally, the energy conservation equation in the solids (windings, core, radiators metal sheets) can be stated as follows

$$\rho C_p(T) \frac{\partial T}{\partial t} = \nabla \cdot (k(T)\nabla T) + \boldsymbol{q} \tag{3}$$

where $k(T)$ is the thermal conductivity, ∇T is the temperature gradient, $\boldsymbol{q}$ is the heat flux density vector and $C_p(T)$ the specific heat. Finally, the energy conservation equation for convective flows of incompressible thermally conducting fluids can be written in the following manner

$$\rho C_p(T) \frac{DT}{Dt} = \nabla \cdot (k(T)\nabla T) \tag{4}$$

where $C_p(T)$ is the specific heat of the fluid at constant pressure. Both the temperature-dependence of the thermal conductivity and specific heat will be defined for the mineral oil and the ester. The coupled oil flow and heat transfer problem is numerically solved with the multiphysics parallel scientific code *Code_Saturne*[26, 27]. The numerical scheme for space discretization of the unsteady Navier-Stokes equations of incompressible viscous fluid flows is based on the finite volume method (FVM) using the second order linear upwind (SOLU) scheme [28]. The coupling of the pressure and velocity fields is done with the SIMPLEC (semi-implicit method for pressure-linked equations consistent) algorithm and a second order Crank-Nicholson time integration scheme is used for the transient simulations [24]. The buoyancy of the oil due to the temperature changes is taken into account in the modelization by considering the temperature dependence of the density $\tilde{\rho}(T)$. For the mineral oil used in this work, the relationship between the density (given in Kg/m^3) and the temperature (given in K) [6] is given by

Journal Pre-proofs

$$\tilde{\rho}_{mineral}(T) = 1067.75 - 0.6376\,T \tag{5}$$

while for the ester oil the relationship is

$$\tilde{\rho}_{ester}(T) = 1109.2 - 0.653\,T \tag{6}$$

Moreover, the dynamic viscosity (μ in Pa s), specific heat (C_p in J/(kg K)) and thermal conductivity (k in W/(m K)) are given by the following equations

$$\mu_{mineral}(T) = 0.08467 - 4 \times 10^{-4}\,T + 5 \times 10^{-7}\,T^2 \tag{7}$$

$$\mu_{ester}(T) = 7.99 - 0.0664\,T + 1.84 \times 10^{-4}\,T^2 - 1.7 \times 10^{-7}\,T^3 \tag{8}$$

$$C_{p_{mineral}}(T) = 807.16 + 3.57\,T \tag{9}$$

$$C_{p_{ester}}(T) = 1273.15 + 1.95\,T \tag{10}$$

$$k_{mineral}(T) = 0.1509 - 7.101 \times 10^{-5}\,T \tag{11}$$

$$k_{ester}(T) = 0.1317 + 4.142 \times 10^{-4}\,T - 8.86 \times 10^{-7}\,T^2 \tag{12}$$

No-slip boundary condition is applied to the velocity field at the solid walls. Since the estimated Rayleigh (Ra) number for the vertical flow is less than $\simeq 10^9$ and the Reynolds (Re) number is 280 for the mineral oil and even less for the ester, it is considered that the oil flow due to natural convection is laminar. Therefore no turbulence model is used in the simulation of the oil flow. The ambient temperature of the air surrounding the transformer is chosen to be $T_{ref} = 30\,°\mathrm{C}$ since according to [4] this is the ambient temperature for rating transformers.

At the initial time $t = 0\,\mathrm{s}$, the velocity of the oil is set to zero in the whole domain, while the oil temperature is set to be uniform and equal to 65 °C. The main objective of using this temperature as initial value is to reduce the number of time steps to attain the steady state with the transient solver. This temperature is estimated by performing an energy balance with a semy-analytic reduced model for the power loss provided by the manufacturer, namely $Q_{t,Exp} = 4250\,\mathrm{W}$, and the heat flux dissipated by the radiators and the oil tank surfaces, considering both convection and radiation.

On the other hand, the heat transfer (convection and radiation) from the walls to the surrounding air is modeled instead of being simulated. This approach is taken since the simulation of the air flow surrounding the transformer would greatly increase the computational cost of the simulations. Therefore, heat transfer coefficients are computed for the top, bottom and lateral surfaces of the transformer using Eq.(13). An empirical equation proposed by [29] is used for the surfaces of the radiators fins

Journal Pre-proofs

$$
\begin{aligned}
h_{conv} &= \mathrm{Nu}\ k/L \\
\mathrm{Pr} &= \mu C_p/k \\
\mathrm{Gr} &= \frac{g\beta|\overline{T_{wall}} - T_{ref}|L^3}{(\mu/\rho)^2} \\
\mathrm{Ra} &= \mathrm{Gr}\ \mathrm{Pr} \\
\mathrm{Nu} &= \left(0.825 + \frac{0.387\mathrm{Ra}^{1/6}}{\left[1 + (0.492/\mathrm{Pr})^{9/16}\right]^{8/27}}\right)^2
\end{aligned}
\tag{13}
$$

which is valid for vertical parallel flat plates, where Pr, Gr, Ra and Nu are the Prandtl, Grashof, Rayleigh and Nusselt numbers for the air, respectively. $\overline{T_{wall}}$ and T_{ref} are the mean wall and external air temperatures, ρ is the air density, L is the length of the surfaces (fins), β is the air thermal expansion coefficient and g is the gravity.

For the top (upward-facing heated plate) and bottom (downward-facing heated plate) surfaces, the following empirical correlations described in [30] are used

$$
\begin{aligned}
\mathrm{Nu}_{top} &= 0.59\mathrm{Ra}^{1/4} \\
\mathrm{Nu}_{bottom} &= 0.27\mathrm{Ra}^{1/4}
\end{aligned}
\tag{14}
$$

where the characteristic length involved in these correlations is $L = area/perimeter$, being *area* the area of the top and bottom surfaces of the transformer oil tank and *perimeter* is the corresponding perimeter.

As stated in [31], the heat transfer due to radiation is another key point in the transformer heat dissipation. In order to estimate the amount of energy transferred to the environment by radiation, a zero-dimensional model of the transformer was considered by solving an energy balance problem. As result of this analysis it is concluded that 17% of the total dissipated energy is due to radiation. Thus, to take into account the radiation, a combined model is used as described in [30]

$$
q = q_{rad} + q_{conv} = (T_{wall} - T_{ref})(h_{rad} + h_{conv}) \tag{15}
$$

The radiation heat transfer coefficient h_{rad} is defined by the following equation

$$
h_{rad} = \sigma\epsilon(T_{wall}^2 + T_{ref}^2)(T_{wall} + T_{ref}) \tag{16}
$$

where ϵ is the emissivity set to 0.94 as defined in [32] for transformers paint and $\sigma = 5.67 \times 10^{-8}\,\mathrm{W/(m^2\,K^4)}$ is the Stefan-Boltzmann constant. To compute h_{rad}, the temperatures T_{wall} and T_{ref} should be expressed in K.

Journal Pre-proofs

5.3. Computation of equivalent thermal conductivities

As it was previously mentioned, it is not feasible to simulate the heat conduction in the windings and magnetic core with a full representation of the copper wires, paper sheet insulation, small oil gaps between the wires, varnish insulation of the wires or each individual steel sheets and sheet coating of the magnetic core. Therefore, to take into account the anisotropy in the heat conduction with a reduced computational cost, a procedure is applied in order to compute equivalent thermal conductivities, which are then introduced into the numerical model. In this work, we follow the ideas presented in [21] and we also perform FVM heat conduction simulations for a representative cell of the particular geometry of the windings and magnetic core under study to compare the estimated values.

Schematic draws of radial cutting planes for the HV and LV windings are shown in Fig. 4. The HV winding is made up of circular cross-section enameled copper wires. There is a craft paper insulation between two wire layers. The wires have diameter $d_C = 1.7\,\mathrm{mm}$ and a varnish insulation which has thickness $e_{Ci} = 0.05\,\mathrm{mm}$. The insulation between wires is made of craft paper which has thickness $e_P = 0.397\,\mathrm{mm}$. The LV winding is made of copper foils of $e_C = 0.5\,\mathrm{mm}$ thickness, while paper sheets are placed as insulator between the copper foils. The paper sheets have thickness $e_P = 0.125\,\mathrm{mm}$.

The HV winding has height $l_{HV} = 260\,\mathrm{mm}$,inner diameter $d_{in,HV} = 261\,\mathrm{mm}$ and radial dimension $e_{HV} = 26\,\mathrm{mm}$. On the other hand, the LV winding has height $l_{LV} = 280\,\mathrm{mm}$, inner diameter $d_{in,LV} = 197\,\mathrm{mm}$ and radial dimension $e_{LV} = 21\,\mathrm{mm}$. The HV winding has 11 wire layers in the radial direction, arranged as 6 wire layers, then the oil cooling ducts and afterwards the remaining 5 wire layers. On the other hand, the LV winding has 26 foil layers in the radial direction, arranged as 13 copper foil layers, then the oil ducts and finally the remaining 13 copper foil layers. To compute the equivalent thermal conductivities in the windings, the following thermal conductivity of each components are used: electrolytic copper $k_C = 394\,\mathrm{W/(m\,K)}$, wire insulation (varnish) $k_{Ci} = 0.26\,\mathrm{W/(m\,K)}$, craft paper interlayer insulation $k_P = 0.47\,\mathrm{W/(m\,K)}$, mineral oil $k_{Oil} = 0.127\,\mathrm{W/(m\,K)}$ at $T_{Oil} = 65\,^\circ\mathrm{C}$ from Eq.(11) and pressboard $k_{Pressboard} = 0.2\,\mathrm{W/(m\,K)}$ taken from [33].

According to the procedure explained in [21], the layout of the different components in the winding has to be clearly defined in order to compute the volume ratio v_j of each material considered in a representative cell of the winding. Since the analysis is carried out on a radial cutting plane of the winding, the volume ratio of material-j (v_j) is defined as the area ratio

$$v_j = A_j / A_{Cell} \tag{17}$$

where A_j is the area of material-j in the cell with total area A_{Cell}. Then it should be satisfied $\sum_j v_j = 1$. For the HV winding, the representative cell is shown in Fig. 11 enclosed by the red dashed line. It includes one quarter of a wire conductor, half of the oil gap between two wires and half the paper insulation thickness. It is assumed for the analysis that the wires are making

contact at one point and the oil velocity in the gaps between paper and wires is very small, so that convective heat transport can be neglected. Moreover, after inspection of the manufacturing process, it is considered that the wires are not aligned but they are arranged in a rhombus or interleaved pattern, as it is shown in Fig. 11. The vertical offset (i.e., in the z-coordinate) between the wire centers is $d_C/2 + e_{Ci}$ and the distance between the centers is $d_C + 2e_{Ci} + e_P$. With this geometric data, it is possible to compute the volume ratios of each element in the representative cell. These volume ratios are: $v_C = 0.629$, $v_{Ci} = 0.076$, $v_{Oil} = 0.090$ and $v_P = 0.204$.

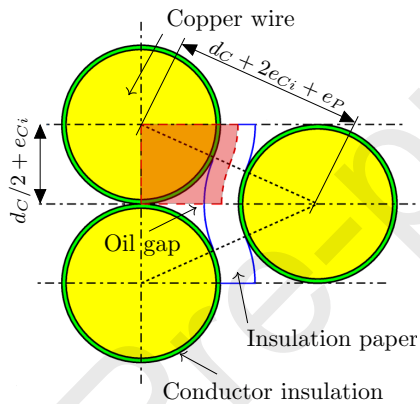

Figure 11: HV winding scheme with representative cell shaded and enclosed by red dashed line.

In the procedure presented in [21], they use an analytic expression for the equivalent conductivity k_e derived by [34], which is valid for stacked cylinders within an insulation matrix, and it is only applicable to two materials, namely conductor and insulator

$$k_e = k_{ins}\frac{(1+v_C)k_C + (1-v_C)k_{ins}}{(1-v_C)k_C + (1+v_C)k_{ins}} \tag{18}$$

If there is more than one insulation material, then it is suggested to amalgamate them into a single compound in the following manner [21]

$$k_{amal} = k_{Oil}\frac{v_{Oil}}{v_{Oil}+v_P+v_{Ci}} + k_P\frac{v_P}{v_{Oil}+v_P+v_{Ci}} + k_{Ci}\frac{v_{Ci}}{v_{Oil}+v_P+v_{Ci}} \tag{19}$$

where k_{amal} is the amalgam thermal conductivity. Then Eq.(18) can be used replacing the insulator by the amalgam

$$k_e = k_{amal}\frac{(1+v_C)k_C + (1-v_C)k_{amal}}{(1-v_C)k_C + (1+v_C)k_{amal}} \tag{20}$$

The equivalent thermal conductivities in the radial and axial direction of the HV winding are $(k_r)_{HV} = (k_z)_{HV} = 1.231\,\mathrm{W/(m\,K)}$. They are computed

taking into account the thermal conductivities of the oil, paper, copper and varnish, their volume ratios calculated from the representative cell shown in Fig. 11, and following the two steps procedure previously described. It should be noted that with this calculation procedure it is not possible to distinguish between the values in the axial and radial directions. On the other hand, the equivalent thermal conductivity in the circumferential direction is computed considering that heat conduction through the different materials is realized in parallel. Therefore

$$(k_\theta)_{HV} = v_C k_C + v_{Oil} k_{Oil} + v_P k_P + v_{Ci} k_{Ci} \tag{21}$$

and $(k_\theta)_{HV} = 205.5\,\mathrm{W/(m\,K)}$.

In addition to the analytic procedure previously explained, numerical simulations were performed in order to validate the computed values. Besides, the analytic procedure provides the same values for $(k_r)_{HV}$ and $(k_z)_{HV}$. Using *Code_Saturne*as numerical solver and following the methodology proposed in [31], a new set of $(k_r)_{HV}, (k_z)_{HV}$ are obtained.

To calculate the radial and axial thermal conductivities, the representative cell denoted with the red shaded area in Fig. 12 (left) is used. To compute the radial thermal conductivity, a temperature difference of 5 K is imposed in the radial direction and the cell boundaries are isolated in the axial direction. On the other hand, to compute the axial thermal conductivity, the boundary conditions are switched. After a mesh convergence analysis, the average heat flux flowing through the representative cell is obtained. Then the equivalent thermal conductivities in both directions are computed from the Fourier law. Using this methodology, it is possible to distinguish the values of the axial and radial directions.

Fig. 12 shows the thermal conductivities of the involved materials on the left, the temperature distribution for the axial case at the center and the temperature distribution for the radial case on the right.

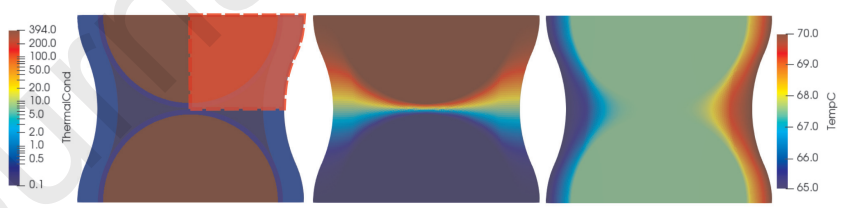

Figure 12: Representative cell of the HV winding enclosed by the red dashed line. Fields of the thermal conductivity (left), the temperature distribution for the axial (center) and radial (right) cases.

Based on these simulations, the radial and axial equivalent thermal conductivities are: $(k_r)_{HV} = 1.26\,\mathrm{W/(m\,K)}$ and $(k_z)_{HV} = 1.31\,\mathrm{W/(m\,K)}$. As can be observed, the magnitude of these values are very close to those computed with the analytic procedure.

Journal Pre-proofs

On the other hand, the estimation of the equivalent thermal conductivities is much simpler in the LV winding since there are no oil gaps between the copper foils and only two materials are considered, namely copper and paper. If the heat conduction problem is analyzed along the radius of the winding, the thermal conductivities are working in series, i.e. the heat should flow first through a copper layer, then through a paper insulation layer, and so on. On the other hand, if the heat conduction problem is analyzed in the circumferential (θ) and axial (z) directions the thermal conductivities are working in parallel since the heat flux is conducted simultaneously along the different layers. Therefore

$$(k_\theta)_{LV} = (k_z)_{LV} = v_C k_C + v_P k_P \tag{22}$$

where $v_C = 0.765$ and $v_P = 0.235$. Then the resulting value is $(k_\theta)_{LV} = (k_z)_{LV} = 301.4\,\mathrm{W/(m\,K)}$. On the other hand

$$(k_r)_{LV} = \frac{k_C k_P}{v_C k_P + v_P k_C} \tag{23}$$

where $v_C = 0.8$, $v_P = 0.2$, and the resulting value is $(k_r)_{LV} = 2.34\,\mathrm{W/(m\,K)}$.

Finally, the equivalent thermal conductivities are computed in the magnetic core. A top view scheme with the dimensions of the core is shown in Fig. 3. The metal sheets are made of Fe-Si grain oriented electrical steel, which has thermal conductivity $k_{steel} = 35\,\mathrm{W/(m\,K)}$. Each sheet is coated on both sides with an inorganic layer based on Phosphate in order to provide good electrical resistance. The coating has thermal conductivity $k_{coating} = 1.04\,\mathrm{W/(mK)}$.

The thickness of each coated sheet is $e_{sheet} = 0.27\,\mathrm{mm}$. Since the height of the core is 85.5 mm, then the number of sheets is 317. The thickness of the coating layer is approximately $e_{coating} = 5\,\mu\mathrm{m}$, therefore the thickness of the steel sheet is $e_{steel} = 0.26\,\mathrm{mm}$. Afterwards, the equivalent thermal conductivities in the directions aligned and normal to the metal sheets are given by

$$k_{Core_aligned} = v_{Steel} k_{Steel} + v_{Coating} k_{Coating} \tag{24}$$

and

$$k_{Core_normal} = \frac{k_{Steel} k_{Coating}}{v_{Coating} k_{Steel} + v_{Steel} k_{Coating}} \tag{25}$$

with $k_{Core_aligned} = 33.7\,\mathrm{W/(m\,K)}$ and $k_{Core_normal} = 16.1\,\mathrm{W/(m\,K)}$. Finally, these values are applied in a cell by cell fashion, considering the appropriate orientation of the cells regarding to the coordinate axes, as it is required by *Code_Saturne*.

6. Results and discussion

In this section, the numerical results computed with the coupled CFD simulations with *Code_Saturne*for both ester and mineral oils, are presented. Additionally, the numerical results are compared to the experimental data provided

Journal Pre-proofs

by Tadeo Czerweny S.A. for the mineral oil and also to the results shown in CIGRE report [35] which covers the experience in service of using synthetic esters, natural esters and silicone fluids in electric transformers.

The experimental measurements provided by the company were obtained for the 315 kVA transformer filled with mineral oil. The provided data are the temperature of components like the HV and LV windings as well as the oil temperature at some characteristic points of the machine. The temperature of the HV and LV windings are estimated following the guidelines established in the IEC 60076-2 [36] standard, which describes an indirect method to measure the average winding temperature. This method is based on measurements of winding resistance at two different temperatures, e.g., a reference temperature and a hot temperature. On the other hand, the top and bottom oil temperatures are measured using thermocouples. The positions of the thermocouples in the transformer are shown in Fig. 13. The top oil temperature is measured at 100 mm below the top surface of the oil tank and the bottom temperature is measured on the fin surface, 30 mm above the bottom boundary of the fin.

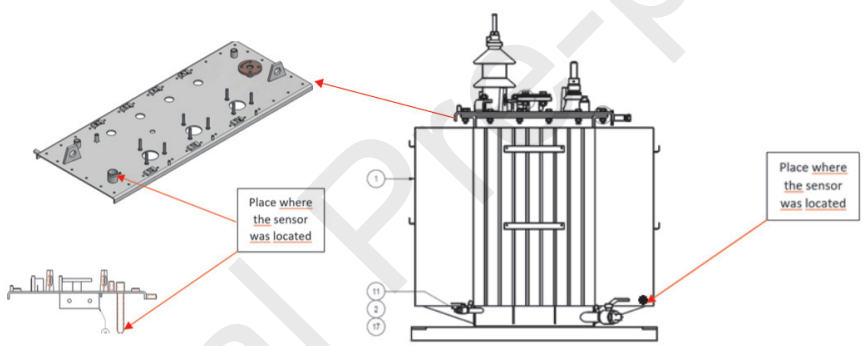

Figure 13: Position of the top (left) and bottom (right) thermocouples.

The last 1200 s (20 min) of the numerical simulations were used to compute the top and bottom time averaged temperatures for both oils. The temperature-time history was analyzed and plotted in Fig. 14. The figure shows that the steady state condition was reached in both cases, because there are no significant temperature changes during this period. For the mineral oil, the time averaged top and bottom temperatures are 72 °C and 57.7 °C, respectively. For the ester oil, the time averaged top and bottom temperatures are 73.5 °C and 56.3 °C, respectively. Therefore, the top temperature of the ester is 1.5 K higher than that of the mineral oil while the bottom temperature of the ester is 1.4 K lower.

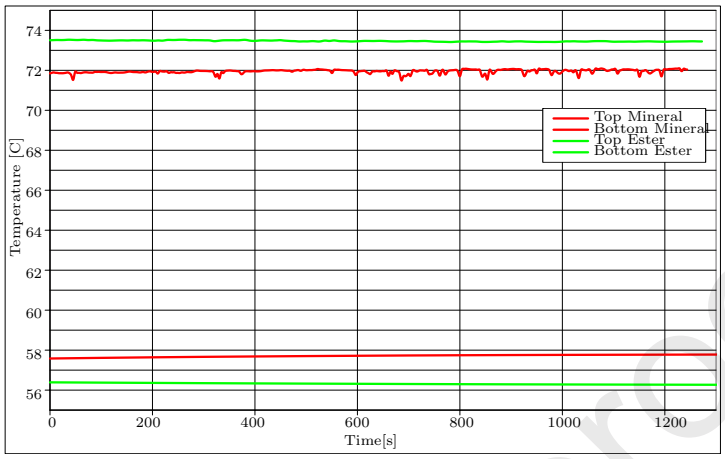

Figure 14: Top and bottom temperatures vs. time (steady state) for mineral and ester oil.

On the other hand, Fig. 15 shows the external temperature distribution together with isolines for 60 °C, 64 °C, 68 °C and 70 °C for both fluids. Additionally, in Fig. 16 the temperature profile is plotted between two fins, along the vertical black solid line indicated in Fig. 15, near the center of the transformer. When using natural ester, higher top and lower bottom temperatures are obtained, thus increasing the temperature gradient along the transformer height, which is shown in the rightmost graph. As it will be shown next, this higher temperature gradient for the ester is mostly due to its higher kinematic viscosity which makes the ester to flow at lower velocities than the mineral oil. Therefore, the natural ester is in contact with the heat source at the windings and magnetic core for a longer period of time than the mineral oil.

Journal Pre-proofs

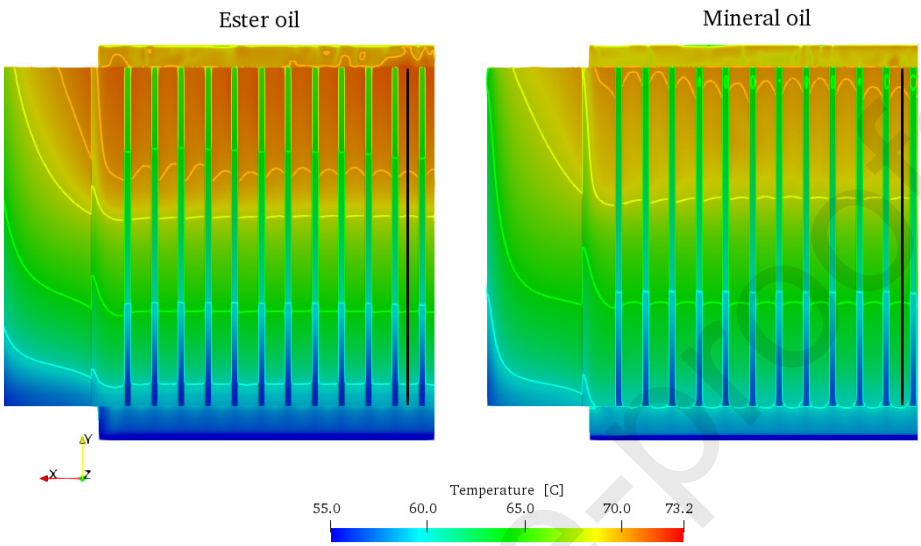

Figure 15: External temperature distribution and temperature isolines corresponding to 60 °C, 64 °C, 68 °C and 70 °C. Black vertical line denotes the position where data is evaluated to build Fig. 16

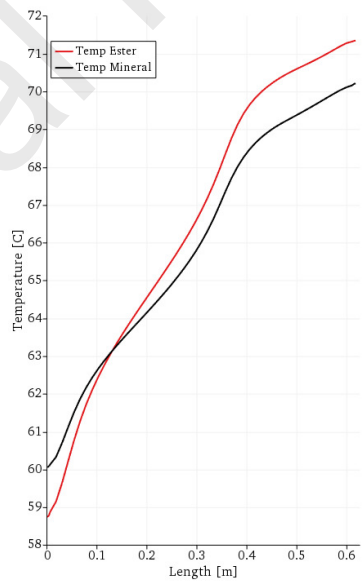

Figure 16: External temperature distribution over the vertical line depicted in Fig. 15

The oil temperature distribution at the midplane section of the transformer is shown in Fig. 17. When natural ester is used as cooling fluid a higher working temperature is obtained, as can be observed in the top region of the transformer and also in the cooling ducts of the windings. The average temperature of the HV winding is 3 °C higher while the LV winding and magnetic core are 2 °C hotter. In Table 1 are listed all the temperatures of the internal components and they are compared to the experimental data.

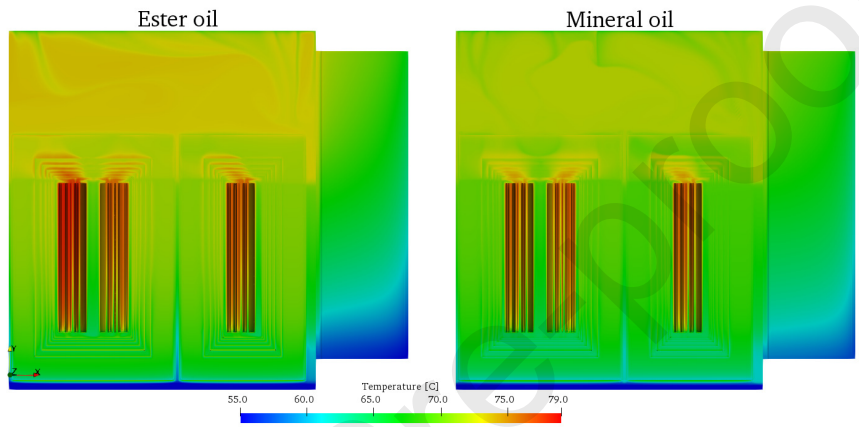

Figure 17: Mid-plane temperature distribution.

Inside the cooling ducts a heat transfer process occurs between the winding internal surfaces and the cooling fluid. The oil flows from the bottom to the top and it is heated during its circulation. In Fig. 18 the fluid temperature is shown in the region of the winding and magnetic core for three cross sections located at the inlet (lower position), middle and outlet (higher position) sections of the winding. It can be seen that a higher temperature is obtained for the ester at the outlet. Also, the temperature of the fluid that is in contact with the windings and magnetic core external surfaces is higher for the ester than for the mineral oil. This is noticeable, for example, in the fluid regions between the two halves of the core or between the core and the inner wall of the winding, at the inlet section. On the other hand, Fig. 19 depicts the fluid temperature evolution along the height of a winding cooling duct. In first place, it can be seen that the mineral oil enters to the winding channel hotter than the natural ester. Secondly, it can be noted that the temperature rise is about 14 °C for the ester and 12 °C for the mineral oil. Lastly, it is noticed that the heat exchange is more significant during the first half of the height due to the higher temperature difference between the oil and the winding surface.

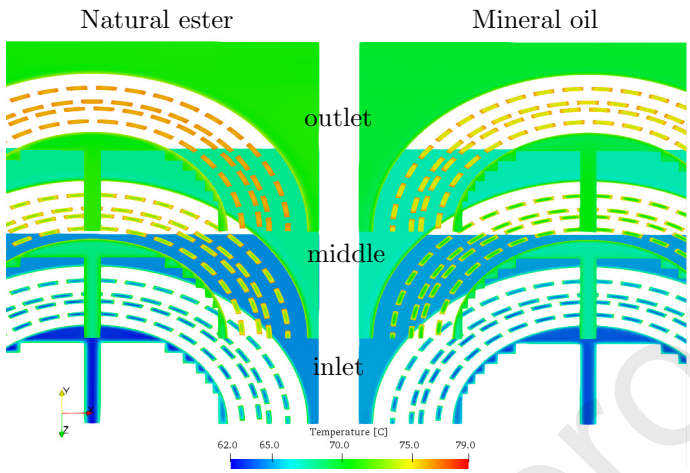

Figure 18: Temperature distribution of the fluid in the windings and magnetic core region at different cross sections along the height of the winding.

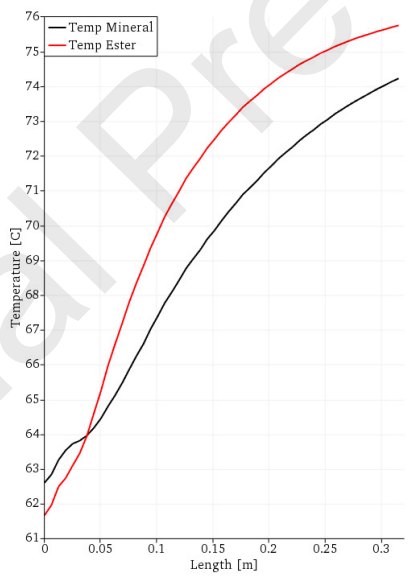

Figure 19: Temperature distribution of the fluid along the height of a winding channel.

Fig. 20 shows the vertical velocity field on a vertical slice of the winding (vertical symmetry plane) for the natural ester and the mineral oil. There are three winding channels in the slice which are indicated by the arrows. The other two regions correspond to the flow in contact with the external surfaces of the winding. On the other hand, Fig. 21 presents the vertical velocity profile for both fluids, in the center of an oil duct, along the height of the winding.

Journal Pre-proofs

From both figures it is clear that the lower kinematic viscosity of the mineral oil produces a higher velocity of the fluid inside the channels. This is also noticeable for the flow field outside of the winding. It can be seen that, for the same fluid, the velocity magnitude is not exactly the same for the three cooling channels. Also, there is an entrance effect of the fluid in the channels, because the velocity is high at the region very close to the entrance, diminishes as the fluid moves upwards and then increases until it goes out of the channel. This behavior is clearly visible in Fig. 21, as well as the fact that the mineral oil flows 20-25% faster than the natural ester, thus increasing the mass flow rate and reducing the winding temperature. Finally, the entrance effect is more important for the mineral oil due to its higher velocity.

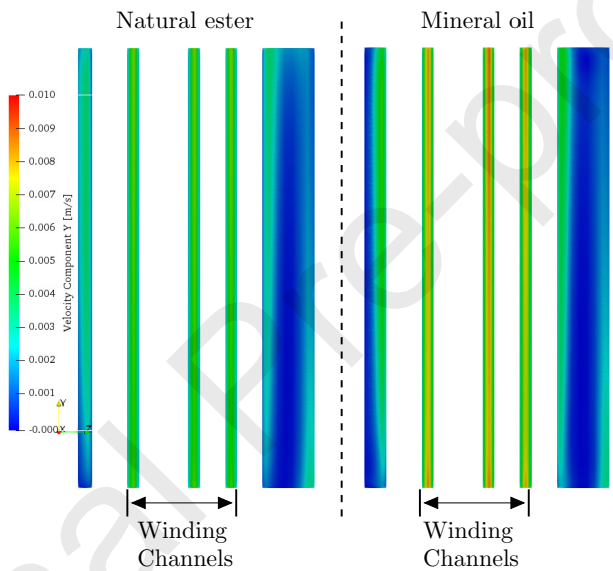

Figure 20: Velocity magnitude field of the fluid inside the winding channels on a vertical cross section (symmetry plane).

Fig. 22 shows the temperature distribution in the windings and magnetic core for the mineral oil and the natural ester as well as the magnitude of the velocity field displayed on two cross sections. One is aligned with the plane perpendicular to the x-axis and the other is aligned with the plane normal to the z-axis. Additionally, streamlines with the velocity vectors are added to the figure to show the oil circulation inside the oil tank and the fins. In both cases, the oil circulation is rather similar, but the velocity is higher for the mineral oil. The maximum velocity magnitude for the ester is almost 0.014 m/s and for mineral oil it is 0.031 m/s. This is an expected result because of the lower kinematic viscosity of the mineral oil. The streamlines also show two distinguishable regions of the flow (i.e., one inside the oil tank and the other inside the fins). It is noticed that the vertical oil flow between the external

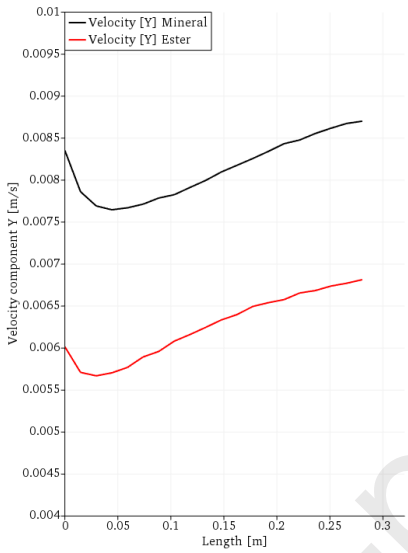

Figure 21: Vertical velocity distribution of the fluid along the height of a winding channel.

surface of the HV winding and the oil tank has very low (almost zero) velocity. Only the oil close to the external surfaces of the windings and inside the cooling channels has a higher velocity.

Journal Pre-proofs

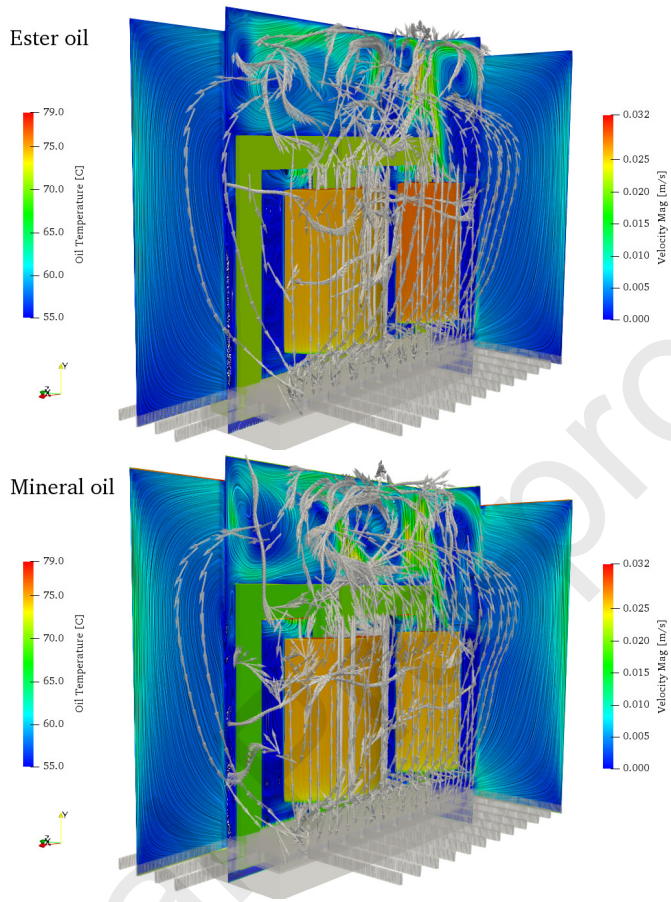

Figure 22: Temperature distribution (windings and magnetic core) and velocity for steady heat dissipation regime. Ester oil (top) and mineral oil (bottom).

It can be observed that the temperature above the winding is higher when ester is used as cooling fluid. This higher temperature can also be noticed at the upper regions of the radiator (see Fig. 15) and magnetic core. Table 1 summarizes the average temperature increments with respect to the ambient temperature assumed for the simulations, namely 30 °C, at different parts of the transformer. Indeed, ΔT_{HV} and ΔT_{LV} are the average temperature increments at the HV and LV windings, ΔT_{oil_top} is the temperature increment of the oil at the top of the tank 100 mm below the top surface, and ΔT_{bot} is measured at the external surface of the radiator fins, 3 mm above of the bottom line of the fins (see Fig.13). On the other hand, ΔT_{oil} is the average oil temperature increment for the complete fluid domain and ΔT_{core} is that for the whole magnetic core.

The values shown in Table 1 confirm that, on average, the oil, windings and core are hotter when the ester oil is used. The windings are approximately 3 K hotter, therefore the HST is also expected to be higher. Moreover, the top oil

	Mineral oil (Num.)	Ester oil (Num.)	Mineral oil (Exp.)
ΔT_{HV}	44.1	47	55.9
ΔT_{LV}	44.3	46.5	52.9
ΔT_{oil_top}	42.0	43.5	45.5
ΔT_{oil_bot}	27.7	26.3	29.9
ΔT_{oil}	38.5	40	37.7
ΔT_{core}	39.5	41.4	–

Table 1: Temperature differences above ambient temperature in the transformer for the ester and mineral oils computed with the simulations.

temperature rise is 1.5 K higher and the bottom oil temperature rise is 1.4 K lower for the ester. This behavior of the temperature in the oil and the windings is in agreement with that reported in [35]. Therein, it is mentioned that for small ONAN cooled transformers up to 5 MVA, the top oil temperature rise when using natural esters is 3 K to 5 K higher, the bottom oil temperature rise is 1 K to 2 K lower and the average winding temperature rise is 1 K to 2 K higher. The third column of the table shows the values of the experimental measurements carried out by Tadeo Czerweny S.A. company during the transformer testing procedure.

When comparing the temperature increase in the HV and LV windings of the numerical simulations with the experimental ones, it can be observed a difference of 12 K for the HV winding and 9 K for the LV winding. Therefore, it seems that the numerical model underestimates the temperature increments at the windings. It is considered that this difference could be due to the following reasons. During the modeling process, several assumptions were applied to the windings, like the estimation of equivalent thermal conductivities to take into account the anisotropic heat conduction, the geometry simplification of the cooling ducts since they are helical in the real device but they are assumed straight in the numerical models in order to reduce computational costs by considering one quarter of the machine. Moreover, some cooling channels are partially blocked in the real machine by additional construction accessories such as the pressboard sheets located between the magnetic core and the windings, as can be observed in Fig. 1. Also in the real device, the oil flow is almost fully blocked by pressboard sheets placed in the gaps between two core loops as it is shown in Fig. 3, but this is not taken into account in the simulations. Finally, the paper sheets used as conductor separators can produce partial or total obstruction at the inlet sections of some cooling channels, thus reducing the oil flow and increasing the temperature.

For the top and bottom oil temperatures, the values are closer to the experimental measurements and it is considered that the difference is related to the modeling of the heat transfer (convection and radiation) with the environment. In the real device, the air between the radiator fins is heated during the oil circulation and the heat transfer coefficient is higher at the inlet region and lower at the outlet. Additionally, near the tank walls the velocity is lower thus reducing

Journal Pre-proofs

the heat transfer coefficient values. In the numerical simulations, the heat transfer coefficient is an average for the given geometry (fin), therefore these specific situations can not be taken into account with the numerical model presented in this work. To avoid these drawbacks, the air surrounding the transformer should be simulated. However, the increase in the computational cost would be rather high if the oil flow, the heat conduction through the solid walls as well as the the air flow due to buoyancy were to be solved in a coupled fashion. Indeed, the air flow surrounding the transformer is turbulent and should be simulated with a turbulence model, which involves additional transport equations to be solved and in some cases requires a detailed mesh close to the walls to accurately solve both the fluid dynamics and the thermal boundary layers. Also, since the oil flow inside the transformer and the external air flow have rather different velocities or characteristic times, the time-dependent solution would be limited by the Courant number of the external air. As a consequence more time steps would be required to reach a steady state solution.

6.1. Conclusions

The current work presents the fluid dynamics and thermal behavior of an ONAN distribution transformer. The focus of the study is on the influence of using a biodegradable ester instead of a mineral oil to cool the device. To this end, 2-D and 3-D EM simulations with FEM models were carried out to estimate the power losses in the windings and magnetic core. Then, the power losses were interpolated from the FEM mesh used in the EM model to FVM meshes used in the CFD model to accurately represent the non-uniform heat distribution in the magnetic core and the windings. In this manner, a more realistic distribution was used instead of averaged values. Equivalent thermal conductivities were estimated in order to take into account the anisotropic heat conduction in the magnetic core and the windings, thus increasing the accuracy of the thermal model. A semi-analytic procedure and numerical simulations with *Code_Saturne*were realized to validate the thermal conductivity values. Afterwards, the coupled thermal and fluid dynamics problem was solved with *Code_Saturne*using an average temperature field as initial condition to reduce the number of time steps needed to attain the thermodynamic steady state of the transformer. The heat dissipated by convection and radiation to the air surrounding the transformer was computed using semi-analytic models and appropriate correlations.

Regarding the power losses, the results obtained with the 3-D EM model were in good agreement with the experimental data provided by the manufacturer, with discrepancies between 4.5% and 2.7% obtained at the typical working temperatures. On the other hand, the simulations carried out with the 3-D CFD model allowed to find that the flow field for the ester and the mineral oil is similar. However, the velocity magnitude for the natural ester is significantly lower than that of the mineral oil because of its higher kinematic viscosity. This is even more noticeable in the cooling channels of the windings. As a consequence, the transformer cooled with the natural ester works at average temperatures higher than with mineral oil. It was also found that the

Journal Pre-proofs

Journal Pre-proofs

increments in the average temperatures in the HV and LV windings due to using ester instead of mineral oil are in good agreement with those reported in [35]. The same conclusion could be drawn for the top and bottom oil temperatures. Even though the temperature increments obtained with the ester are accepted by insulation standards because of its much higher water saturation point and thus extended operation life of the transformer, it is important to mention that the heat removal in the winding ducts could be improved by increasing the heat exchange area of the channels and also avoiding their partial obstruction due to inaccuracies in the manufacturing process.

Acknowledgments

This work has received funding from European Union's Horizon 2020 research and innovation program under the Marie Sklodowska-Curie grant agreement No 823969 (BIOTRAFO project of Research and Innovation Staff Exchanges RISE, check https://www.biotrafo.unican.es/, @biotrafo); Consejo Nacional de Investigaciones Científicas y Técnicas (CONICET, Argentina, grant PIP 11220150100588 CO); Universidad Nacional del Litoral (UNL, Argentina, grant CAI+D-2016-50420150100112LI); Agencia Nacional de Promoción Científica y Tecnológica (ANPCyT, Argentina, grants PICT-2018-01607, PICT-2018-02920, PICT-2016-0708).

The efforts in the research development were organized and carried out in the following manner: a) Garelli, L., Rios Rodriguez, G., Storti, M. and Smolka, J.: i) CFD simulations with *Code_Saturne*, ii) Coupling of the EM and CFD models in order to transfer the power losses from the first to the second one, iii) Analysis and computation of the equivalent thermal conductivities to take into account anisotropic heat conduction; b) Krzysztof, K., Lasek, P. and Stepien, M.: i) EM simulations with Ansys Maxwell, ii) Coupling of the EM and CFD models; c) Pessolani, F. and Amadei, M.: i) Experimental data supply, ii) Geometry, Manufacturing and Technical data supply, iii) Knowledge about technical details in the manufacturing process.

This work was performed with *Free Software Foundation/GNU-Project* resources such as GNU–Linux OS, GNU–GFortran, GNU–Octave, GNU–Git, GNU-GCC, and GNU–GIMP, as well as other open source resources such as Salome, ParaView, *Code_Saturne*, OpenFoam and LaTeX.

Additionally, the authors made use of the computer cluster "Seshat", which is part of the computer center of CIMEC. This computer center is integrated into the Sistema Nacional de Computación de Alto Desempeño (SNCAD), which is a joint project of Ministerio de Ciencia, Tecnología e Innovación Productiva (MINCyT) and Consejo Interinstitucional de Ciencia y Tecnología (CICyT), Argentina.

References

[1] P. Rozga, Properties of new environmentally friendly biodegradable insulating fluids for power transformers, in: 1st Annual International Interdisciplinary Conference, AIIC, Portugal, 2013.

[2] Cargill Inc., Reference Data R2020 - Envirotemp^{TM}FR3^{TM}Fluid Behavior in Cold Temperature Environments (October 2017).
URL https://www.cargill.com/doc/1432076502222/r2020-fr3-fluid-behavior-in-cold-tds.pdf

[3] IEC60076-14 Ed.1.0. b:2013 Power transformers - Part 14: Liquid-immersed power transformers using high-temperature insulation materials, International Electrotechnical Commission Standard, Geneva.

[4] IEEE Std C57.91-2011 - IEEE Guide for Loading Mineral-Oil-Immersed Transformers and Step-Voltage Regulators, IEEE Standards Association.

[5] M. Kim, S. M. Cho, J.-K. Kim, Prediction and evaluation of the cooling performance of radiators used in oil-filled power transformer applications with non-direct and direct-oil-forced flow, Experimental Thermal and Fluid Science 44 (0) (2013) 392 – 397. doi:http://dx.doi.org/10.1016/j.expthermflusci.2012.07.011.

[6] A. Santisteban, F. O. Fernández, I. F. F. Delgado, A. Ortiz, C. J. Renedo, Thermal analysis of natural esters in a low-voltage disc-type winding of a power transformer, in: 2017 IEEE 19th International Conference on Dielectric Liquids (ICDL), 2017, pp. 1–4. doi:10.1109/ICDL.2017.8124698.

[7] H. Nabati, J. Mahmoudi, A. Ehteram, Heat transfer and fluid flow analysis of power transformer's cooling system using CFD approach, Chemical Product and Process Modeling 4 (43). doi:http://dx.doi.org/10.2202/1934-2659.1428.

[8] G. Ríos Rodriguez, L. Garelli, M. Storti, D. Granata, M. Amadei, M. Rossetti, Numerical and experimental thermo-fluid dynamic analysis of a power transformer working in ONAN mode, Applied Thermal Engineering 112 (2017) 1271 – 1280. doi:https://doi.org/10.1016/j.applthermaleng.2016.08.171.
URL http://www.sciencedirect.com/science/article/pii/S1359431116315290

[9] M. Tsili, E. Amoiralis, A. Kladas, A. Souflaris, Power transformer thermal analysis by using an advanced coupled 3-D heat transfer and fluid flow FEM model, International Journal of Thermal Sciences 53 (0) (2012) 188 – 201. doi:http://dx.doi.org/10.1016/j.ijthermalsci.2011.10.010.

[10] F. Torriano, P. Picher, M. Chaaban, Numerical investigation of 3-D flow and thermal effects in a disc-type transformer winding, Applied Thermal

Engineering 40 (0) (2012) 121 – 131. doi:http://dx.doi.org/10.1016/j.applthermaleng.2012.02.011.

[11] S. Paramane, K. Joshi, W. Van der Veken, A. Sharma, CFD Study on Thermal Performance of Radiators in a Power Transformer: Effect of Blowing Direction and Offset of Fans, IEEE Transactions on Power Delivery 29 (6) (2014) 2596–2604. doi:10.1109/TPWRD.2014.2347292.

[12] S. Paramane, W. Van der Veken, A. Sharma, A coupled internal–external flow and conjugate heat transfersimulations and experiments on radiators of a transformer, Applied Thermal Engineering 103 (2016) 961 – 970. doi:https://doi.org/10.1016/j.applthermaleng.2016.04.164.

[13] L. Garelli, G. Ríos Rodriguez, M. Storti, D. Granata, M. Amadei, M. Rossetti, Reduced model for the thermo-fluid dynamic analysis of a power transformer radiator working in ONAF mode, Applied Thermal Engineering 124 (2017) 855 – 864. doi:https://doi.org/10.1016/j.applthermaleng.2017.06.098.
URL http://www.sciencedirect.com/science/article/pii/S1359431117300868

[14] Z. Radakovic, M. Sorgic, Basics of detailed thermal-hydraulic model for thermal design of oil power transformers, IEEE Transactions on Power Delivery 25 (2) (2010) 790–802. doi:10.1109/TPWRD.2009.2033076.
URL https://ieeexplore.ieee.org/document/5382493

[15] H. M. R. Campelo, L. F. Braña, X. Lopez Fernandez, Thermal hydraulic network modelling performance in real core type transformers, 2014 International Conference on Electrical Machines (ICEM) (2014) 2275 – 2281doi:10.1109/ICELMACH.2014.6960502.
URL https://ieeexplore.ieee.org/document/6960502

[16] R. Bouhaddiche, S. Bouazabia, I. Fofana, Thermal modelling of power transformer, IEEE 19th International Conference on Dielectric Liquids (ICDL) (2017) 1 – 4doi:10.1109/ICDL.2017.8124676.
URL https://ieeexplore.ieee.org/document/8124676

[17] T. Park, S. Han, Numerical analysis of local hot-spot temperatures in transformer windings by using alternative dielectric fluids., Electrical Engineering 97 (2015) 261 – 268. doi:10.1007/s00202-015-0335-4.

[18] L. Raeisian, H. Niazmand, E. Ebrahimnia-Bajestan, P. Werle, Feasibility study of waste vegetable oil as an alternative cooling medium in transformers, Applied Thermal Engineering 151 (2019) 308 – 317. doi:https://doi.org/10.1016/j.applthermaleng.2019.02.010.
URL https://www.sciencedirect.com/science/article/abs/pii/S1359431118358587

[19] M. M. Salama, D.-E. A. Mansour, M. Daghrah, S. M. Abdelkasoud, A. A. Abbas, Thermal performance of transformers filled with environmentally friendly oils under various loading conditions, International Journal of Electrical Power & Energy Systems 118 (2020) 105743. doi:https://doi.org/10.1016/j.ijepes.2019.105743.
URL http://www.sciencedirect.com/science/article/pii/S0142061519328893

[20] Raising knowledge and developing technology for the design and deployment of high-performance power transformers immersed in biodegradable fluids "biotrafo", https://www.biotrafo.unican.es/.
URL https://www.biotrafo.unican.es/

[21] N. Simpson, R. Wrobel, P. Mellor, Estimation of equivalent thermal parameters of impregnated electrical windings, IEEE Transactions on Industry Applications 49 (6) (2013) 2505 – 2515. doi:10.1109/TIA.2013.2263271.

[22] Salome: The Open Source Integration Platform for Numerical Simulation, https://www.salome-platform.org/.
URL https://www.salome-platform.org/

[23] The open source CFD toolbox, snappyHexMesh - OpenFOAM: User Guide v1912.
URL https://www.openfoam.com/documentation/guides/latest/doc/guide-meshing-snappyhexmesh.html

[24] Code_saturne documentation.
URL https://www.code-saturne.org/cms/documentation/v60

[25] P. Le Quéré, R. Masson, P. Perrot, A Chebyshev collocation algorithm for 2D non-Boussinesq convection, Journal of Computational Physics 103 (2) (1992) 320 – 335. doi:https://doi.org/10.1016/0021-9991(92)90404-M.
URL http://www.sciencedirect.com/science/article/pii/002199919290404M

[26] Code_Saturne an open source CFD software, http://code-saturne.org.
URL http://code-saturne.org

[27] F. Archambeau, N. Méchitoua, M. Sakiz, Code Saturne: A finite volume code for the computation of turbulent incompressible flows - Industrial applications, International Journal on Finite Volumes 1 (1) (2004) http://www.latp.univ–mrs.fr/IJFV/spip.php?article3.
URL https://hal.archives-ouvertes.fr/hal-01115371

[28] S. Norris, A parallel Navier-Stokes solver for natural convection and free surface flow, Ph.D. Thesis, Department of Mechanical Engineering, Sydney (2000).

Journal Pre-proofs

[29] S. Churchill, H. Chu, Correlating equations for laminar and turbulent free convection from a vertical plate, Int. J. Heat and Mass Transfer 18 (1975) 1323–1329.

[30] Ashrae, 2009 ASHRAE Handbook - Fundamentals (SI Edition), ASHRAE Handbook Fundamentals, American Society of Heating, Refrigerating and Air-Conditioning Engineers, Inc., 2009.

[31] J. Smolka, A. Nowak, Experimental validation of the coupled fluid flow, heat transfer and electromagnetic numerical model of the medium-power dry-type electrical transformer, International Journal of Thermal Sciences 47 (10) (2008) 1393 – 1410. doi:https://doi.org/10.1016/j.ijthermalsci.2007.11.004.
URL http://www.sciencedirect.com/science/article/pii/S1290072907002414

[32] Testo se & co., https://www.testo.com/en-TH/services/knowledgeable-thermography-emissivity-table.
URL https://www.testo.com/en-TH/services/knowledgeable-thermography-emissivity-table

[33] R. Wittmaack, Thermal design of power transformers via CFD, in: E. Oñate, J. Oliver, A. Huerta (Eds.), 11th. World Congress on Computational Mechanics, 5th. European Conference on Computational Mechanics, 6th. European Conference on Computational Fluid Dynamics, 2015.
URL https://pdfs.semanticscholar.org/c131/5c21a7dbfbc0efdc1d4501b78b54f2eee919.pdf

[34] Z. Hashin, S. Shtrikman, A variational approach to the theory of the effective magnetic permeability of multiphase materials, Journal of Applied Physics 33 (10) (1962) 3125–3131. arXiv:https://doi.org/10.1063/1.1728579, doi:10.1063/1.1728579.
URL https://doi.org/10.1063/1.1728579https://aip.scitation.org/doi/10.1063/1.1728579

[35] M. Russel, Experiences in service with new insulating liquids, CIGRE Technical Brochure A2.35, CIGRE (2010).
URL https://e-cigre.org/publication/436-experiences-in-service-with-new-insulating-liquids

[36] IEC60076-2 Ed. 3.0 b:2011 Power Transformers - Part 2: Temperature Rise For Liquid-immersed Transformers, International Electrotechnical Commission Standard, Geneva.

Journal Pre-proofs